



Exploring the mechanism of Stephania tetrandra S. Moore in the treatment of cisplatin resistance against ovarian cancer through integration of network pharmacology and molecular docking

Yuanyuan Zhong, MDa,b, Shanshan Cai, PhD, DVMc, Chunyue Fang, MDa,d, Wei Dai, MDa,*

Abstract

Cisplatin resistance is a major contributor to treatment failure in ovarian cancer (OC). This study investigates the mechanisms of action and therapeutic targets of Stephania tetrandra S. Moorefor cisplatin-resistant OC. OC datasets were obtained from the gene expression omnibus database, and differentially expressed genes were identified through weighted gene co-expression network analysis. Cisplatin resistance-related targets were screened using the GeneCards, OMIM, and MsigDB databases, while active components of S tetrandra were retrieved from the TCMSP, ETCM, and BATMAN databases. Commonly shared genes between these 2 sets were selected for further analysis. A protein-protein interaction network was constructed using the STRING database, and 4 machine learning algorithms were integrated to identify core targets. Binding affinities were evaluated by molecular docking with AutoDock Vina. Molecular dynamics simulations were then conducted to assess the stability of the ligandtarget complexes. We performed ADMET analysis to assess the pharmacokinetic properties and drug-likeness of S tetrandra. Machine learning algorithms further identified 8 core targets including threonine tyrosine kinase (TTK), AURKA, B-cell lymphoma 2, vitamin D receptor, NFKB1, cyclin dependent kinase 1, DNMT1, and SMAD7. Gene ontology and Kyoto Encyclopedia of Genes and Genomes pathway enrichment analyses revealed that these targets were significantly enriched in pathways such as the PI3K-AKT, cell cycle regulation, p53 signaling pathway, and platinum resistance pathway. Receiver operating characteristic curve analysis demonstrated diagnostic potential for all genes except SMAD7 (AUC = 0.603 < 0.7). Immune infiltration analysis indicated a positive correlation between AURKA/TTK expression and M0/M1 macrophage infiltration (P <.05). Molecular dynamics simulations demonstrated that hesperidin, cissamine and tetrandrine exhibited strong binding affinities toward AURKA, vitamin D receptor, and TTK. Future studies are encouraged to focus on the experimental validation of these compounds and delve deeper into the possible mechanisms of drug resistance, aiming to improve their therapeutic effectiveness and real-world applicability.

Abbreviations: BCL2 = B-cell lymphoma 2, CDK1 = cyclin dependent kinase 1, DEG = differentially expressed gene, GO = gene ontology, HBonds = hydrogen bonds, KEGG = Kyoto Encyclopedia of Genes and Genomes, MDS = molecular dynamics simulation, OC = ovarian cancer, Rg = radius of gyration, RMSD = root mean square deviation, RMSF = root mean square fluctuation, ROC = receiver operating characteristic, SASA = solvent accessible surface area, TTK = threonine tyrosine kinase, VDR = vitamin D receptor, WGCNA = weighted gene co-expression network analysis.

Keywords: cisplatin resistance, machine learning, molecular dynamics simulation, network pharmacology, ovarian cancer, *Stephania tetrandra* S. Moore

YZ and SC contributed to this article equally.

This work was supported by the Scientific Research Fund of Education Department of Yunnan Province (2025J0784).

The authors have no conflicts of interest to disclose.

The datasets generated during and/or analyzed during the current study are available from the corresponding author on reasonable request.

This study was based on publicly available data from open-access databases, which do not involve human subjects, animal experiments, or identifiable personal information, neither informed consent nor approval of the ethics committee is

Supplemental Digital Content is available for this article.

^a Department of Pharmacy, The Third People's Hospital of Yunnan Province, Kunming, Yunnan, China, ^b Yunnan Cancer Hospital, The Third Affiliated Hospital of Kunming Medical University, Peking University Cancer Hospital Yunnan, Kunming, Yunnan, China, ^c Division of Biomedical and Life Sciences, Faculty of Health and Medicine, Lancaster University, Lancaster, UK, ^d College of Pharmacy, Dali University, Dali, Yunnan, China. * Correspondence: Wei Dai, Department of Pharmacy, The Third People's Hospital of Yunnan Province, Kunming, Yunnan 650011, China (e-mail: 24190285@qq.com).

Copyright © 2025 the Author(s). Published by Wolters Kluwer Health, Inc. This is an open-access article distributed under the terms of the Creative Commons Attribution-Non Commercial License 4.0 (CCBY-NC), where it is permissible to download, share, remix, transform, and buildup the work provided it is properly cited. The work cannot be used commercially without permission from the journal.

How to cite this article: Zhong Y, Cai S, Fang C, Dai W. Exploring the mechanism of Stephania tetrandra S. Moore in the treatment of cisplatin resistance against ovarian cancer through integration of network pharmacology and molecular docking. Medicine 2025;104:46(e45860).

Received: 28 July 2025 / Received in final form: 15 August 2025 / Accepted: 9 October 2025

http://dx.doi.org/10.1097/MD.0000000000045860

1. Introduction

Ovarian cancer (OC) represents a leading gynecologic malignancy globally, with disproportionately high incidence rates observed across Eastern/Northern Europe and Southeast Asia.^[1] Although its incidence has been gradually declining, OC remains associated with the highest mortality rate among gynecologic cancers.^[2] It is characterized by rapid progression, low survival rates, high heterogeneity,^[3] and a significant propensity for drug resistance. Patients often present with nonspecific clinical symptoms such as abdominal discomfort and bloating. At first clinical presentation, 70% of OC patients already manifest regionally advanced or metastatic disease,^[4] highlighting considerable challenges in early detection. Once diagnosed at an advanced stage, the disease frequently progresses to metastasis and develops drug resistance.^[5]

The primary treatment strategies for OC include tumor cytoreductive surgery and platinum-based combination chemotherapy, [6] with cisplatin typically serving as the first-line chemotherapeutic agent. [7] Cisplatin exerts its cytotoxic effects primarily through the formation of DNA adducts, [8] causing cell cycle arrest in the G2 phase, followed by the suppression of growth and the induction of apoptotic cell death. However, the development of resistance to platinum-based drugs, the mainstay of OC therapy has significantly hindered effective tumor eradication,[9] creating a major bottleneck in treatment and necessitating improvements in the 5-year survival rate among OC patients.[10] Following an initial favorable response to platinum-based regimens, the majority of patients ultimately acquire secondary resistance, typically after experiencing several recurrences,[11] resulting in progressively shorter progressionfree survival. Ultimately, platinum resistance profoundly affects the overall prognosis of all OC patients.

Natural compounds derived from animals, plants, and microorganisms have attracted increasing attention due to their potent antitumor activity, [12] low toxicity, [13] and multitargeting [14] properties. Preclinical evidence confirms their capacity to suppress metastatic dissemination, trigger programmed cell death, and reverse radio-chemotherapy resistance. [15,16]

Stephania tetrandra S. Moore, a perennial vine of the Menispermaceae family, contains abundant alkaloidal components. This plant exhibits anti-inflammatory, neuroprotective, and antiviral properties and possesses a long-standing history of therapeutic application for multiple disorders, including cancer, edema, rheumatoid arthritis, rheumatism, hypertension, and hyperglycemia. These therapeutic attributes provide a scientific basis for considering *S tetrandra* as a potential candidate for treating cisplatin-resistant OC. However, the precise molecular mechanisms underlying its role in reversing cisplatin resistance remain poorly understood, necessitating further multidisciplinary and analytical investigations.

In this study, machine learning-assisted network pharmacology was implemented to discern bioactive constituents in *S tetrandra* and their molecular targets relevant to overcoming cisplatin resistance in OC. Molecular docking validation was also performed. The purpose of this study is to establish a solid theoretical foundation for the clinical application of *S tetrandra*, while also putting forward new, efficient, and low-toxicity combination treatment strategies for OC.

2. Materials and methods

2.1. OC dataset collection

The gene expression omnibus (https://www.ncbi.nlm.nih.gov/geo/) served as the source for the OC datasets, which were retrieved employing the query criteria "ovarian cancer, Homo sapiens." Two datasets were selected: GSE14407, which includes 12 normal control samples and 12 OC samples, and GSE38666, which contains 20 normal samples and 25 OC samples. The 2

datasets mentioned above were merged and standardized using the Sva R package.

2.2. Construction of a WGCNA

The R package "WGCNA" was utilized to carry out weighted gene co-expression network analysis (WGCNA).^[20] First, hierarchical clustering was applied to detect and remove outlier samples. Subsequently, the pickSoftThreshold function was employed to determine the optimal soft threshold for establishing a scale-free network. An adjacency matrix was created and subsequently converted into a topological overlap matrix. Constructed gene tree diagrams and module colors using different degrees. Module-trait associations were quantified by correlating eigengene values with differential expression profiles across sample cohorts.

2.3. Identification of genes with differential expression in OC

Normalization of the GSE63142 expression matrix was performed with the "Sva" package in R. Differentially expressed genes (DEGs) were detected with the "limma" package in R, applying thresholds of $llog_2$ Fold Changel > 1 and P < .05. Heatmaps were constructed utilizing the "pheatmap" R package. Volcano plots were generated with the "ggplot2" package.

2.4. Acquisition of cisplatin resistance-related targets in OC

To identify cisplatin resistance-related targets, we conducted a search on the GeneCards website (https://www.genecards.org/)^[21] and OMIM (https://omim.org/) databases using the keyword "cisplatin resistance." The MsigDB database (https://www.gsea-msigdb.org/gsea/msigdb) provided additional target information. The target genes were identified as the intersection of OC DEGs, WGCNA hub genes, and cisplatin resistance-related genes using the Venn2.2.1 online tool (https://bioinfogp.cnb.csic.es/tools/venny/index.html). It is important to note that the criteria for screening DEGs were set as llog₂ Fold Changel > 1 and *P* < .05. The WGCNA gene set primarily included the modules MEbrown, MEpink, MEred, and MEturquoise. Only genes present in all 3 sets proceeded to subsequent analysis.

2.5. Acquisition of active components and targets from S tetrandra

BATMAN-TCM (https://bionet.ncpsb.org.cn/batman-tcm/#/ home) is a comprehensive database of traditional Chinese medicine (TCM), aiming to collect known and predicted connections between the components of TCM and target proteins.[22] It is specifically designed to understand the pharmacological mechanisms of TCM and identify active ingredients for disease treatment. The BATMAN-TCM 2.0 database was employed to screen active ingredients of S tetrandra with a score cutoff >0.84. Additionally, compounds were screened from the TCMSP database (https://www.tcmsp-e.com/) using selection criteria of oral bioavailability ($OB \ge 30\%$) and drug-likeness ($DL \ge 0.18$). The ETCM repository^[23] (https:// www.tcmip.cn/ETCM/index.php/Home/) was systematically searched to retrieve bioactive constituents of S tetrandra. Putative biological targets of these phytochemicals were identified using SwissTargetPrediction (https://www.swisstargetprediction.ch/), a web-based prediction platform. In the end, all predicted targets underwent integration and deduplication processes to yield the definitive list of targets associated with S tetrandra.

2.6. Intersection target acquisition for cisplatin-resistant OC treated with S tetrandra

The overlapping targets between *S tetrandra*-related targets and cisplatin-resistant OC-related targets were identified using a Venn diagram (available at https://www.bioinformatics.com.cn), and these intersecting targets were selected for further analysis.

2.7. The construction of protein–protein interaction (PPI) network

Overlapping targets were analyzed via the STRING platform^[24] (https://string-db.org/), with species specification to Homo sapiens and interaction score cutoff set at 0.4. Network visualization was performed with cytoscape (version 3.10.2). Topological analysis was conducted using the CytoNCA plugin. The size of the text, the shade of the color, and the size of the nodes were adjusted based on the degree value. The larger the degree value, the larger the text, the darker the color, and the larger the node, which also indicates that the importance of this node in the protein interaction network is higher.

2.8. Integrated GO term and KEGG pathway enrichment

Enrichment profiling for gene ontology (GO) terms and Kyoto Encyclopedia of Genes and Genomes (KEGG) pathways was conducted with configured R packages (org.Hs.e.g.db, colorspace, stringi, DOSE, clusterProfile, pathview, ggplot2, limma), utilizing significance thresholds of P value cutoff = .05 and q value cutoff = 0.05. The GO function analysis mainly encompassed 3 categories of biological process (BP), cellular component (CC) and molecular function (MF). Significantly enriched terms (P < .05) were ranked by P-value, with the top ten entries visualized.

2.9. Machine learning model construction

The intersecting gene expression matrix from GSE14787 was utilized to develop a machine learning model via the "caret" "radom Forest" "kernlab" "xgboost"package in R. Algorithms included random forest, support vector machine, generalized linear model, and eXtreme Gradient Boosting. The dataset was partitioned into a training set (70%) and test set (30%) via stratified sampling using createDataPartition. A 5-fold repeated cross-validation was implemented to minimize overfitting and optimize hyperparameters. Key tuned parameters were detailed in Table S1, Supplemental Digital Content, https://links.lww.com/MD/Q637. Model performance was evaluated using residual analysis and receiver operating characteristic (ROC) curves, leading to the identification of the top 10 variables as key genes.

2.10. Single-gene analysis

ROC curves were generated for each pivotal gene to assess diagnostic accuracy. Genes exhibiting an AUC value exceeding 0.7 were deemed potentially valuable for disease diagnosis purposes. To visualize the differential expression patterns of the previously identified key genes between patient and control cohorts, we employed boxplots created using the R package "ggplot2."

2.11. Analysis of immune infiltration

For the purpose of ascertaining the relative abundance of immune cells within the samples, the OC expression data were analyzed using CIBERSORT. The mRNA expression matrix was examined via the CIBERSORT R script, which was retrieved from the CIBERSORT website and utilized CIBERSORT L22 as the reference. To compare immune cell proportions between groups, the Wilcoxon rank-sum test was applied, defining statistical significance at P < .05.

2.12. Molecular docking validation

All small-molecule 3D conformations utilized in this work originated from PubChem. This publicly available resource can be accessed at https://pubchem.ncbi.nlm.nih.gov/. SYBYL-X 2.0 was utilized to perform molecular optimization under the following conditions: tripos force field application, Gasteiger-Hückel charge calculation, 10,000-iteration maximum, and 0.005 kcal/(mol A) energy convergence criterion; all other parameters maintained default configurations. The RCSB PDB repository (https://www.rcsb.org/) served as the source for the target macromolecule's 3-dimensional atomic coordinates. Molecular preparation of receptors was conducted in MGLTools 1.5.6 (Windows version), involving water molecule elimination, metal ion removal, and other essential preprocessing steps prior to PDBQT format conversion. AutoDock Vina 1.1.2 (https://vina.scripps.edu/) was used to evaluate docking affinity between ligands and proteins. Structural renderings of docking complexes were generated with discovery studio in conjunction with PyMOL.

2.13. Molecular dynamics simulation

Molecular dynamics simulation (MDS) were implemented in GROMACS 2022 to investigate. Force field topology derivation employed dual resources: GROMACS-native pdb2gmx tool, AutoFF web server for ligand parameterization. During the simulation, the molecular parameters of the receptor protein were based on the CHARMM36m force field, [25] while those of the ligand were based on the CGenff force field. A 1nm TIP3P-type cubic water box was added around the system for solventization. Ions were added to the system using the gmx genion tool to achieve electrical neutrality. Long-range electrostatic interactions were handled using the particle mesh Ewald method, with a cutoff distance of 1 nm. All bonds were constrained using the SHAKE algorithm, and the MDS was performed using the Verlet leapfrog algorithm with an integration step size of 1 fs. The system was energy-optimized prior to the MDS. The energy minimization process included 3000 steps of steepest descent optimization followed by 2000 steps of conjugate gradient optimization. The optimization steps are as follows: first, the solute is constrained, and the water molecules are minimized; then, the counterions are constrained, and the system is minimized; finally, the entire system is minimized without constraints. The simulation was conducted at a temperature of 310K under constant pressure in an NPT system, with a simulation time of 100 ns. During the simulation, the tools g-root mean square deviation (RMSD), g-root mean square fluctuation (RMSF), ghydrogen bonds (HBonds), g-radius of gyration (Rg), and g-solvent accessible surface area (SASA) were applied to compute the RMSD, RMSF, HBonds, Rg, and SASA in a respective manner.

2.14. ADMET properties prediction

To predict the ADMET properties of *S tetrandra* components, we utilized the SwissADME online database (https://swissadme. ch) to evaluate their pharmacokinetic characteristics, including absorption, distribution, metabolism, and excretion, as well as potential toxicity risks. This database offers comprehensive predictions of key pharmacokinetic parameters, drug-likeness, and pharmacological properties. Compounds exhibiting favorable ADMET profiles were prioritized for further investigation and potential experimental validation.

3. Results

3.1. WGCNA analysis of OC

Hierarchical clustering was performed on the study samples using WGCNA to detect outliers and remove abnormal samples. Next, a scale-free network was constructed by selecting

an optimal soft threshold ($\beta = 20$, $R^2 = 0.946$), as shown in Figure 1A. Subsequently, the adjacency matrix was constructed and transformed into a topological overlap matrix. Gene dendrograms and module colors were produced according to varying degrees (Fig. 1B). In total, all genes were clustered into 13 modules. Modules colored blue indicated negative correlation with OC traits, while red modules showed positive correlation; the strength of the correlation was mirrored by the intensity of the color. Among them, MEblack, MEblue, MEgreen, MEgrey, and MEtan exhibited significantly positively correlated with OC, but their correlation coefficients were all <0.5, whereas MEbrown, MEpink, MEred, MEturquoise, and MEyellow were significantly negatively correlated with OC; the correlation coefficients of MEbrown, MEpink, MEred, and MEturquoise were -0.77, -0.54, -0.8, and -0.85 in decibels, so these 4 modules were selected for subsequent analysis (Fig. 1C).

Filtering the individual module genes by gene importance and gene-module correlation, with filtering thresholds set at geneSigFilter = 0.5 and moduleSigFilter = 0.8. The results showed that MEbrown was a gene cluster related to 234 core genes including ACTR10, CRNDE, FAM213A, GCA, PPAP2A, etc (Fig. 1D); MEpink was a gene cluster related to 146 core genes including LIPT1, VPS37A, ZC3H14,

SELT, ZZZ3, KLHL7, etc (Fig. 1E); MEred was a gene cluster related to 209 core genes including B-cell lymphoma 2 (BCL2), SPAG9, MAGI2-AS3, ATG2B, DTWD1, etc (Fig. 1F); METurquoise was a gene cluster related to 341 core genes including SH3BP5, ARMCX1, CAV1, GAS1, RTN4, SNX3, PLSCR4, etc (Fig. 1G). In summary, a total of 1619 module genes were obtained.

3.2. Differential gene analysis for OC

Using the "limma" R package, DEGs in OC were identified under the criteria of $llog_2$ Fold Changel > 1 and P < .05. A total of 3173 DEGs were detected (Fig. 2A), with 132 upregulated ones among them, for instance, PTH2R, SOX17, ZIC1, and MUC1, as well as 1848 downregulated genes such as ITLN1, TCEAL7, SGCG, ADH1B, and OGN (Fig. 2B).

3.3. Acquisition of cisplatin-resistant targets in OC

The keyword "Cisplatin resistance" was used to search the GeneCards database, resulting in 4868 candidate genes. Among these, 331 targets with a relevance score >10 were selected. Additionally, 50 cisplatin-resistant targets were retrieved from

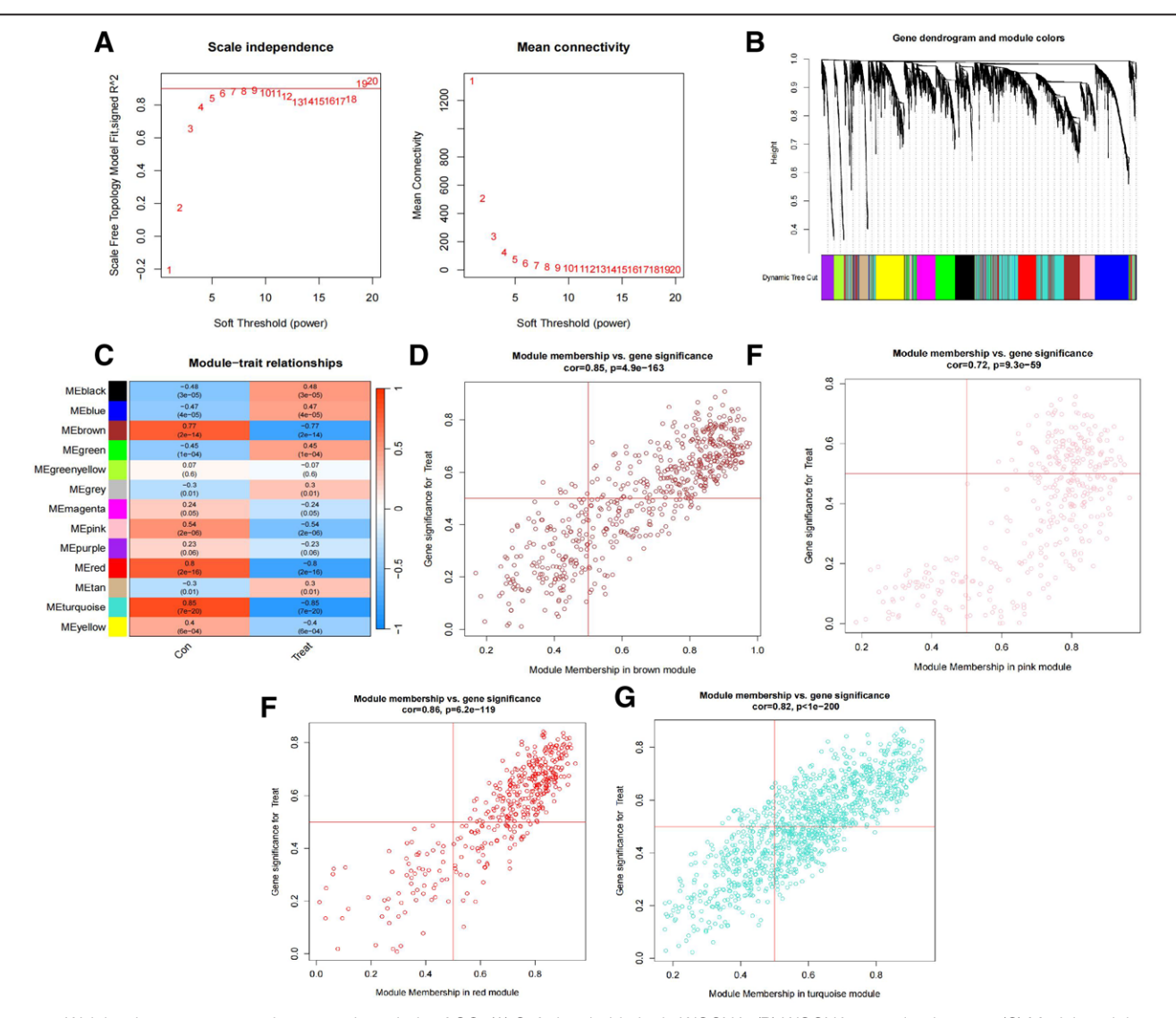


Figure 1. Weighted gene co-expression network analysis of OC. (A) Soft threshold plot in WGCNA. (B) WGCNA gene dendrogram. (C) Module-trait heatmap illustrating correlations between modules and OC. (D–G) Significant gene screening maps for the MEbrown, MEpink, MEred, and MEturquoise modules, respectively. OC = ovarian cancer, WGCNA = weighted gene co-expression network analysis.

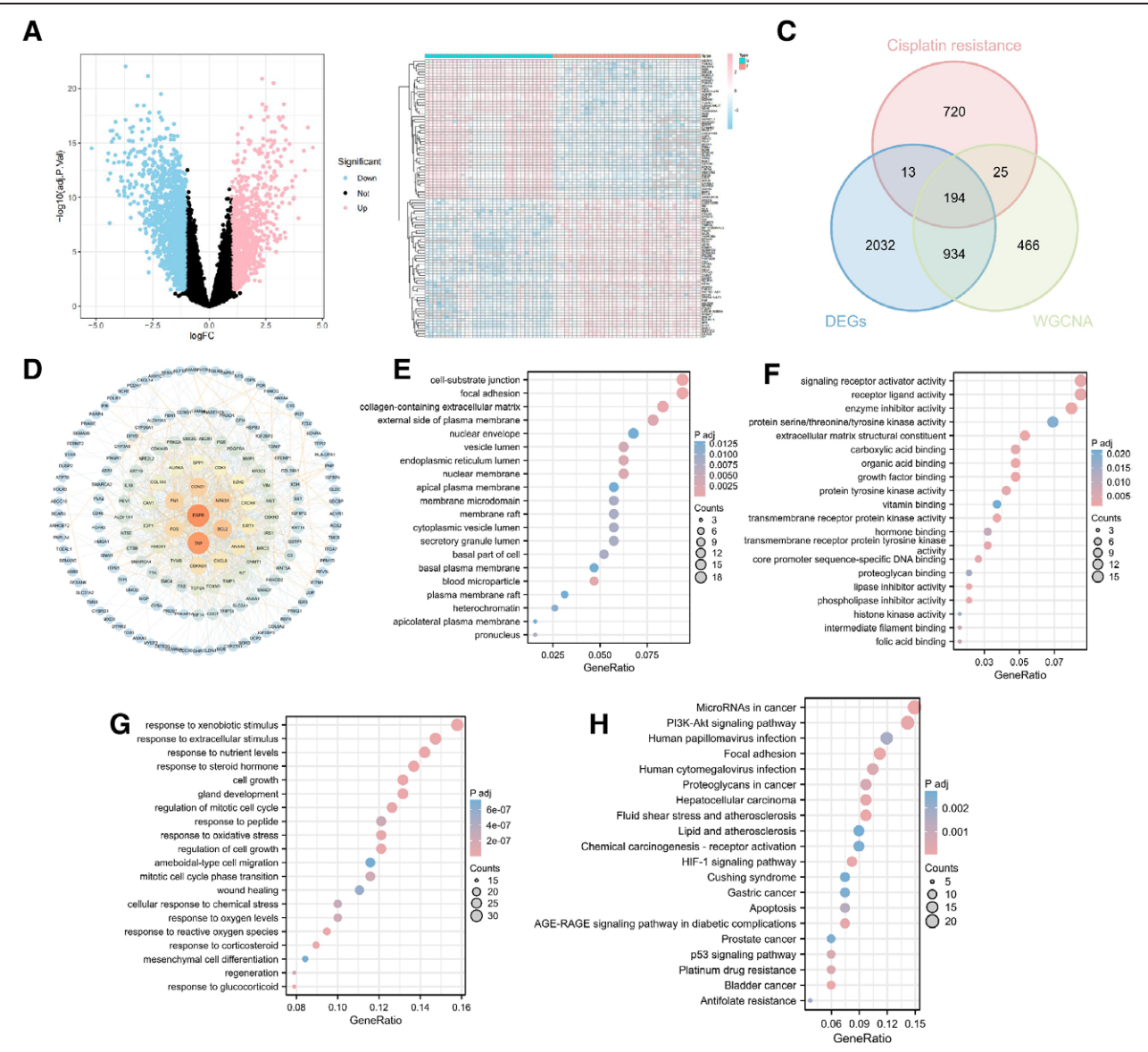


Figure 2. Mechanistic analysis of cisplatin resistance in OC. (A) Volcano plot of differentially expressed genes in OC. (B) Heatmap of differentially expressed genes in OC. (C) Identification of cisplatin-resistant targets in OC. (D) Protein-protein interaction network of cisplatin-resistant targets in OC. (E) GO enrichment analysis of cisplatin-resistant genes in OC (biological process). (F) GO enrichment analysis of cisplatin-resistant genes in OC (cellular component). (G) GO enrichment analysis of cisplatin-resistant genes in OC. (GO = gene ontology, KEGG = Kyoto Encyclopedia of Genes and Genomes, OC = ovarian cancer.

the OMIM database. In the MsigDB database, gene sets associated with cisplatin resistance were collected based on the following terms: BRACHAT_RESPONSE_TO_CISPLATIN, KANG_CISPLATIN_RESISTANCE_DN, KANG_CISPLATIN_RESISTANCE_UP, KERLEY_RESPONSE_TO_CISPLATIN_DN, KERLEY_RESPONSE_TO_CISPLATIN_UP, LI_CISPLATIN_RESISTANCE_DN, LI_CISPLATIN_RESISTANCE_UP, TSUNODA_CISPLATIN_RESISTANCE_DN, WANG_CISPLATIN_RESPONSE_AND_XPC_DN,WANG_CISPLATIN_RESPONSE_AND_XPC_UP, WHITESIDE_CISPLATIN_RESISTANCE_DN, and WHITESIDE_CISPLATIN_RESISTANCE_UP. A total of 628 cisplatin-resistant genes were obtained from MsigDB.

After consolidating gene entries from 3 distinct databases and eliminating redundant entries, a total of 952 unique cisplatin-resistant genes were identified. Subsequently, an intersection analysis was performed among these 952 cisplatin-resistant genes, 173 OC DEGs, and 1619 modular genes derived from WGCNA. This process yielded 194 OC-associated cisplatin-resistant genes (Fig. 2C).

3.4. Protein-protein interaction network construction for cisplatin resistance in OC

PPI network was constructed based on the 194 identified cisplatin-resistant genes using the STRING database and visualized with Cytoscape. In this network, nodes were color coded according to their degree values: blue for low-degree nodes, light yellow for medium-degree nodes, and yellow for high-degree hub targets. The resulting network consisted of 167 nodes and 1110 interactions, with EGFR, TNF, BCL2, CCND1, and NF-κB1 identified as the top-ranked hub genes based on degree value (Fig. 2D).

3.5. Functional enrichment analysis of cisplatin resistance in OC

To delineate molecular mechanisms underlying cisplatin resistance in OC, we performed functional enrichment analyses using GO and KEGG pathway databases. GO analysis revealed a total of 1468 BP terms, including response to xenobiotic stimulus, response to steroid hormone, response to extracellular stimulus, response to nutrient levels, response to corticosteroid, and gland development (Fig. 2E). CC analysis identified 75 entries, such as focal adhesion, cell-substrate junction, collagen-containing extracellular matrix, blood microparticle, and nuclear membrane (Fig. 2F). MF analysis included 96 categories, with key terms such as phospholipase inhibitor activity, extracellular matrix structural constituent, enzyme inhibitor activity, growth factor inhibitor activity, growth factor binding, and organic acid binding (Fig. 2G).

KEGG pathway enrichment identified 93 significantly enriched pathways, including MicroRNAs in cancer, bladder cancer, fluid shear stress and atherosclerosis, focal adhesion, HIF-1 signaling pathway, Hepatocellular carcinoma, PI3K-Akt signaling pathway, AGE-RAGE signaling pathway in diabetic complications, human cytomegalovirus infection, Platinum drug resistance, and p53 signaling pathway (Fig. 2H).

3.6. Acquisition of active components and targets from S tetrandra

Relevant potential active ingredients along with their respective target molecules were gathered from a variety of databases, including TCMSP (2 compounds, 40 targets), ETCM (4 compounds, 29 targets), and BATMAN-TCM (4 compounds, 43 targets). A total of 10 unique bioactive compounds were identified. SwissTargetPrediction was used to predict additional targets, and after integrating all data sources and removing duplicates, a final list of 402 targets for *S tetrandra* was obtained.

3.7. Identification of cisplatin-resistant targets regulated by S tetrandra in OC

An intersection analysis was performed between the 194 cisplatinresistant targets in OC and the 402 targets of *S tetrandra*, yielding 21 overlapping targets that may represent potential therapeutic targets for reversing cisplatin resistance in OC (Fig. 3A).

3.8. Protein–protein interaction network analysis of S tetrandra-regulated cisplatin resistance in OC

The 21 overlapping target molecules were uploaded to the STRING database, and a PPI network was constructed via visualization with Cytoscape. Topological analysis revealed that CCND1, NF-κB1, and BCL2 exhibited high connectivity and centrality in the network, implying that they play key roles in regulating the impacts of *S tetrandra* on cisplatin resistance (Fig. 3B).

3.9. Identification of core components in S tetrandra for treating cisplatin-resistant OC

To explore the relationships among herbal components, targets, pathways, and disease mechanisms, a herb-component-target-pathway-disease network was constructed using cytoscape. This network contained 93 nodes and 260 edges (Fig. 3C). Topological analysis identified PRKCA, NF-κB1, and BCL2 as key regulatory hubs involved in the reversal of cisplatin resistance by *S tetrandra* (Fig. 3D). Among the active components, tetrandrine, thal-rugosine, β-sitosterol, hesperetin, and (+)-2-*N*-methyltetrandrine interacted with the highest number of targets, with 10, 7, 6, 6, 6, 6, 6 target associations, respectively (Fig. 3E).

3.10. Functional enrichment analysis of cisplatin resistance in OC regulated by S tetrandra

To further clarify the biological roles linked to the 21 intersecting genes that are modulated by *S tetrandra*, functional

enrichment analysis was performed. GO analysis revealed 864 BP terms, including gland development, peptidyl-threonine phosphorylation, peptidyl-threonine modification, reproductive structure development, and reproductive system development, etc (Fig. 4A). CC analysis identified 35 categories, such as spindle, cyclin-dependent protein kinase holoenzyme complex, spindle microtubule, serine/threonine protein kinase complex, and protein kinase complex, etc (Fig. 4B). MF analysis included 82 entries, with key terms such as histone kinase activity, protein serine/threonine/tyrosine kinase activity, nuclear receptor activity, ligand-activated transcription factor activity and steroid binding, etc (Fig. 4C).

KEGG pathway enrichment identified 62 significantly enriched pathways, primarily including MicroRNAs in cancer, Prostate cancer, AGE-RAGE signaling pathway in diabetic complications, chemical carcinogenesis-receptor activation, PI3K-Akt signaling pathway, gastric cancer, EGFR tyrosine kinase inhibitor resistance, small cell lung cancer, focal adhesion, HIF-1 signaling pathway, cell cycle, measles, hepatocellular carcinoma, melanoma, non-small cell lung cancer, p53 signaling pathway, glioma, chronic myeloid leukemia, gap junction, and Epstein-Barr virus infection, etc (Fig. 4D). Detailed information for each enrichment term is presented in Figure 4E.

3.11. Machine learning identification of core targets of S tetrandra in reversing cisplatin resistance in OC

Four distinct machine learning algorithms were utilized to screen for key regulatory targets from among the 21 intersecting genes. The models were constructed using the R package "caret," and model performance was evaluated using residual analysis and ROC curves. Results showed that all 4 models exhibited low residuals (Fig. 5A, B), and the area under the ROC curve (AUC) exceeded 0.7 for each method. Notably, random forest and support vector machine achieved AUC values of 1 (Fig. 5C). The top 10 features from each model were selected as candidate core genes (Fig. 5D).

3.12. Expression and diagnostic value analysis of core targets

Since all 4 machine learning models demonstrated acceptable performance, an intersection analysis was conducted among the top-ranked genes from each model. Genes present in at least 3 models were defined as core targets: threonine tyrosine kinase (TTK), AURKA, SMAD7, BCL2, DNMT1, vitamin D receptor (VDR), NF-κB1, and cyclin dependent kinase 1 (CDK1; Fig. 6A). The center coordinates of the core target points are presented in Table 1. Expression analysis revealed that SMAD7 showed no significant difference between OC and normal tissues, whereas AURKA, CDK1, DNMT1, TTK, and VDR were upregulated in OC samples. In contrast, BCL2 and NF-κB1 were downregulated (Fig. 6B). ROC analysis indicated that all core genes except SMAD7 had diagnostic potential (AUC > 0.7; Fig. 6C). Line graphs displaying expression trends of core genes as shown in Figure 6D.

3.13. Core targets immune infiltration correlation analysis

Figure 7A demonstrates the percentage of 22 immune cell types within the samples, the highest percentage was T cells CD4 memory resting. Figure 7B demonstrates the difference in expression abundance of 22 immune cells in normal and OC groups. Figure 7C demonstrated the difference in expression of 22 immune cells in normal and OC groups, for example, macrophage M1 and 0 expression was significantly upregulated in the OC group. Figure 7D demonstrates the correlation between

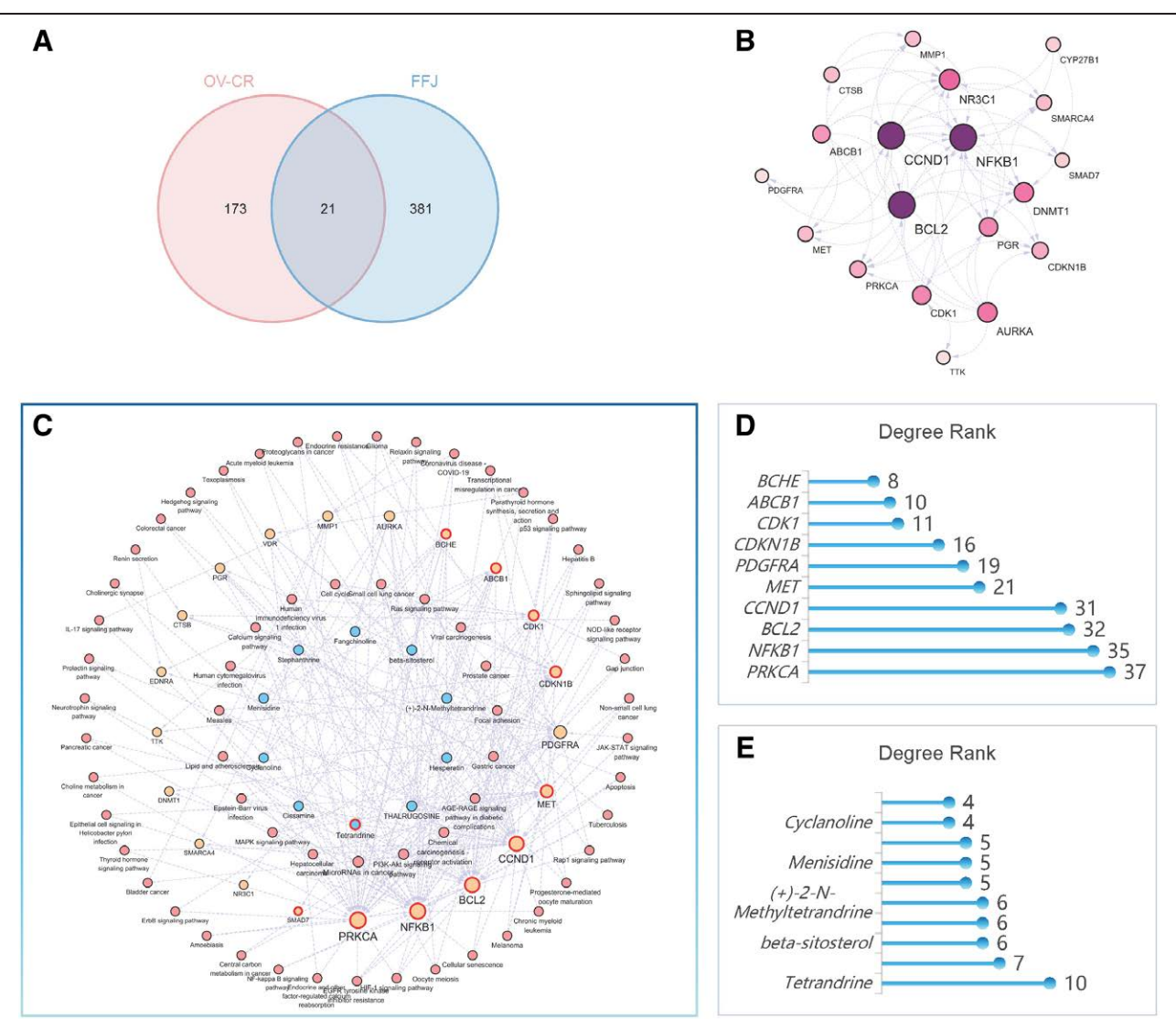


Figure 3. Core components of *S tetrandra* defense against cisplatin-resistant OC. (A) Venn diagram showing the intersection of cisplatin-resistant genes and *S tetrandra*-related targets in OC. (B) Protein–protein interaction network of cisplatin-resistant targets regulated by *S tetrandra*. (C) The network of herbs, components, targets and pathways of *S tetrandra* in the treatment of cisplatin-resistant OC. (D) Ranking of degree values for target proteins in the network. (E) Ranking of degree values for herbal components in the network. OC = ovarian cancer.

immune cells, red is negative correlation, * indicates significant difference, you can select the immune cells you are interested in analyzing. Figure 7E shows the correlation analysis between core targets and immune cells, for example, AURKA showed significant positive correlation with macrophage M0 and 1.

3.14. Molecular docking validation of core target and components

Based on machine learning results, the following 8 core targets were selected for molecular docking validation: TTK, AURKA, SMAD7, BCL2, DNMT1, VDR, NF-κB1, and CDK1. Binding affinity between these targets and active components of *S tetrandra* was assessed. Generally, binding energy <-7 kcal/mol indicates strong interaction. Results showed that all targets, except VDR and BCL2, exhibited binding energies below this threshold. Among the compounds tested, (+)-2-*N*-methyltetrandrine, hesperidin, menisidine, tetrandrine, and thalrugosine displayed strong binding affinities to multiple targets. The binding energies of the respective compounds are presented in Figure 8A. We have visualized the interactions between hesperidin and AURKA, VDR and cissamine, as well as TTK and tetrandrine.

Hesperidin formed HBonds with ASP274, LYS162, and LYS258 of AURKA, along with van der Waals interactions with GLY140, LYS141, LEU129, and Pi-alkyl interactions with LEY263 and VAL147 (Fig. 8B). Cissamine formed van der Waals with ILE271, SER237, and PHE150 of VDR, Pi-alkyl interactions with VAL300, LEU230, and LEU233, and Pi-sigma interactions with HIS305 and TRP286 (Fig. 8C). Additionally, tetrandrine formed van der Waals with ASP664, GLY534, and ASN652 of TTK, Pi-alkyl interactions with VAL539, ILE633, ALA651 (Fig. 8D).

3.15. Molecular dynamics simulation

RMSD is a good indicator of the conformational stability of proteins and ligands, as well as a measure of the degree of deviation of atomic positions from their initial positions. The smaller the deviation, the better the conformational stability. Therefore, RMSD was used to evaluate the equilibrium of the simulated system. As shown in Figure 9A, the VDR-cissamine, TTK-tetrandrine, and AURKA-hesperidin complex systems all reached equilibrium after 5 ns, with final values fluctuating around 2.94, 2.26, and 2.20 Å, respectively. Therefore, the small

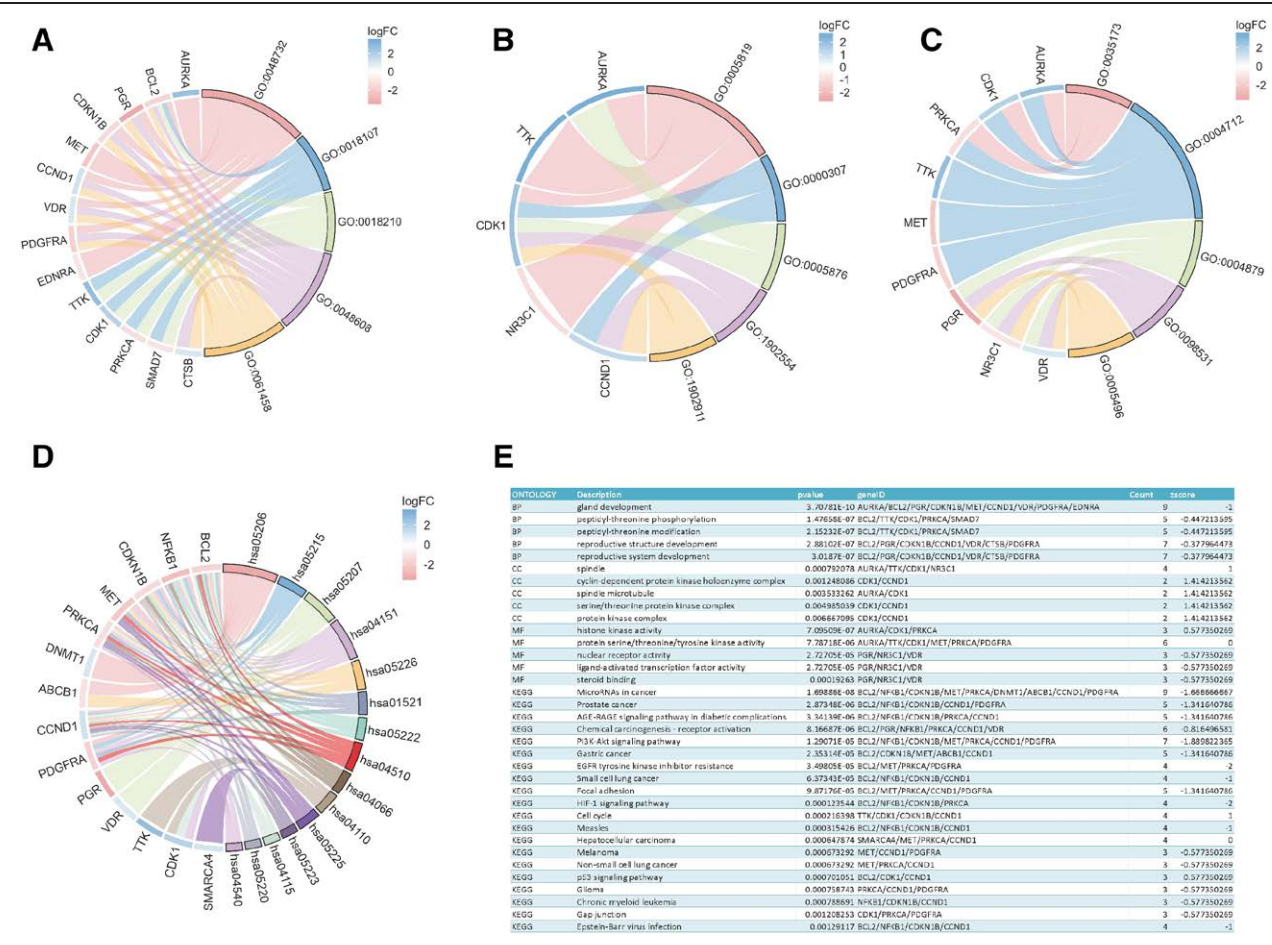


Figure 4. Functional enrichment analysis of cisplatin resistance in OC regulated by *S tetrandra*. (A) GO enrichment analysis (biological process). (B) GO enrichment analysis (cellular component). (C) GO enrichment analysis (molecular function). (D) KEGG pathway enrichment analysis. (E) Summary of significant enrichment results. GO = gene ontology, KEGG = Kyoto Encyclopedia of Genes and Genomes, OC = ovarian cancer.

molecules cissamine, tetrandrine, and hesperidin exhibit high stability when bound to the target proteins VDR, TTK, and AURKA, respectively.

Rg quantifies alterations in the global conformation and measures the compactness of protein structures, larger Rg changes indicate greater system expansion. The VDR-cissamine, TTK-tetrandrine, and AURKA-hesperidin complex systems exhibit slight fluctuations during motion, indicating that the small molecule-target protein complexes undergo conformational changes during motion (Fig. 9B).

SASA is an indicator for assessing protein surface area. In this simulation, the solvent-accessible surface area between the target protein and small molecules was calculated (Fig. 9C). The results showed that after the VDR-cissamine, TTK-tetrandrine, and AURKA-hesperidin receptors bound to their ligands, the SASA of the complexes did not change significantly, indicating that ligand binding has a minimal impact on protein structure.

HBonds play a crucial role in ligand-protein binding. The number of HBonds between small molecules and target proteins during the kinetic process is shown in Figure 9D. The number of HBonds between the VDR-cissamine small molecule and the target protein ranges from 0 to 4, with most complexes having approximately 2 HBonds. In most cases, there is 1 HBond between the TTK-tetrandrine small molecule and the target protein. The number of HBonds between the AURKA-hesperidin small molecule and the target protein ranges from 0 to 4, with most complexes having approximately 3 HBonds. This indicates that this ligand has good hydrogen bonding interactions with the target protein.

RMSF can indicate the flexibility of amino acid residues in a protein. As shown in Figure 9E, the RMSF values of the VDR-cissamine, TTK-tetrandrine, and AURKA-hesperidin complexes are relatively low (mostly below 2.2 Å), indicating lower flexibility and higher stability.

To conclude, the VDR-cissamine, TTK-tetrandrine, and AURKA-hesperidin complex systems exhibit stable binding, and the complexes demonstrate good hydrogen bonding interactions. Consequently, the small molecules cissamine, tetrandrine, and hesperidin exhibit good binding interactions with VDR, TTK, and AURKA.

3.16. ADMET profile analysis

We conducted a comprehensive assessment of the ADMET profiles of the compounds identified in our study. The detailed data were presented in Table S2, Supplemental Digital Content, https://links.lww.com/MD/Q637. The evaluation of drug-likeness using Lipinski's rule of 5 revealed distinct profiles among the compounds. For hesperidin, its molecular weight was 302.28 Da, the log *P* value was 1.91, indicating appropriate lipophilicity. It had 6 hydrogen bond acceptors and 3 donors, which were also within the defined limits. The topological polar surface area was 96.22, suggesting good oral bioavailability potential. Tetrandrine, its molecular weight was 622.75 Da, which was slightly above the typical limit. The log *P* value was 5.49, it had 8 hydrogen bond acceptors and 0 donors, and had poor solubility.

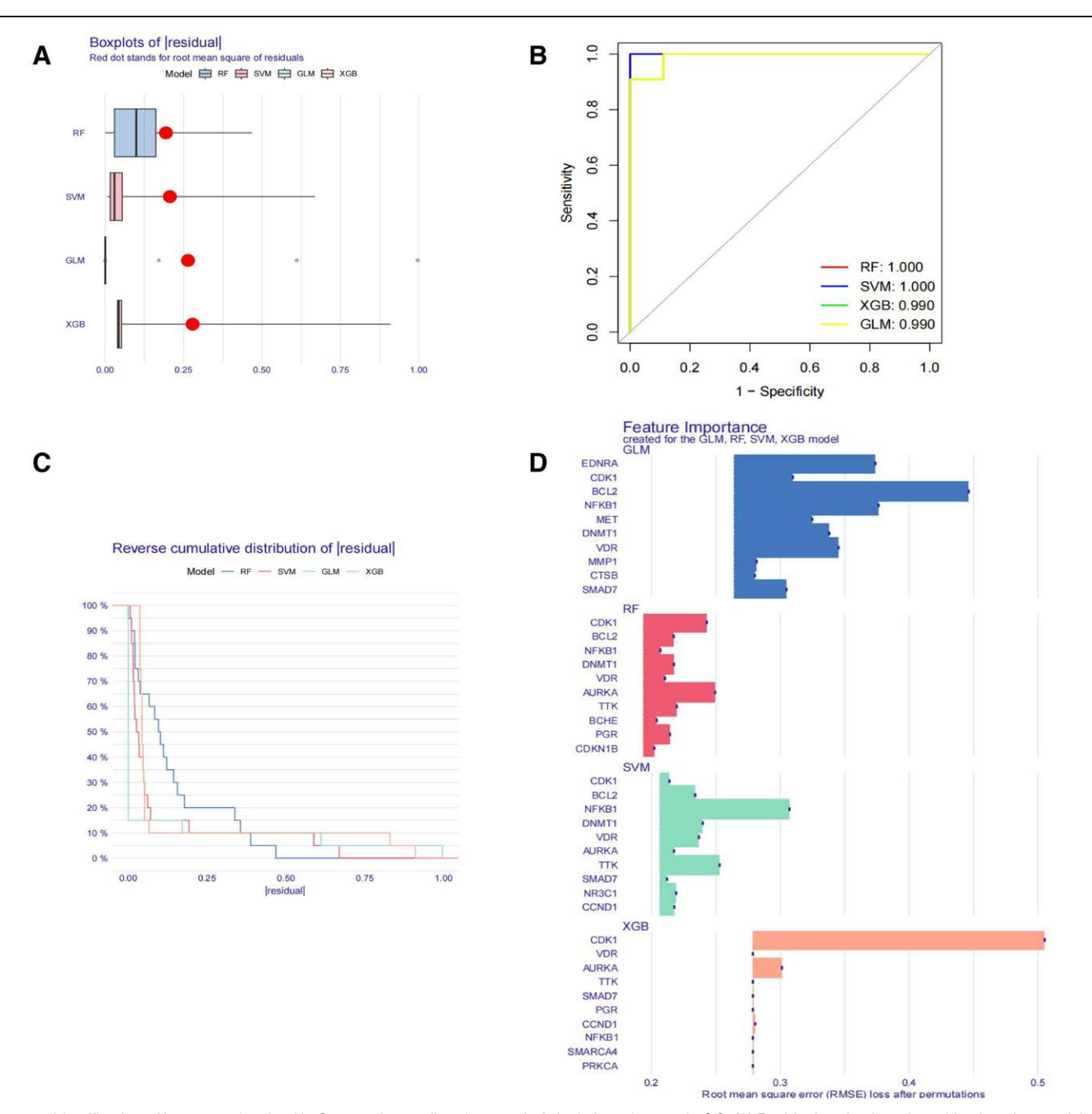


Figure 5. Identification of key genes involved in *S tetrandra*-mediated reversal of cisplatin resistance in OC. (A) Residual evaluation of machine learning models. (B) Residual distribution across models. (C) ROC curve evaluation. (D) Ranking of feature importance for identifying core genes. OC = ovarian cancer, ROC = receiver operating characteristic.

4. Discussion

Although progress has been made in the early detection and multimodal treatment of OC, chemoresistance remains a major contributor to disease recurrence and mortality. Therefore, identifying novel agents that can restore tumor sensitivity to cisplatin without inducing significant toxicity to normal tissues is crucial for improving patient outcomes. Recently, natural compounds have shown promise in suppressing tumor invasion, metastasis, and resistance to therapy.^[26,27] Hence, exploring bioactive components from natural products represents a viable approach to surmounting cisplatin resistance in OC.

In this study, we systematically investigated the molecular mechanisms underlying *S tetrandra*-mediated reversal of cisplatin resistance by integrating network pharmacology, bioinformatics, and molecular docking approaches. Initially, to identify potential

targets associated with *S tetrandra*, we adhered to database protocols and compiled target molecules from 5 distinct repositories, resulting in 402 unique *S tetrandra*-associated targets after eliminating duplicates. To explore therapeutic targets for OC, we selected the GSE14407 and GSE38666 datasets from the gene expression omnibus database as they cover OC samples. Using WGCNA, we identified key molecules associated with OC progression. To obtain cisplatin-resistant targets and mitigate biases from single-dataset reliance, we integrated 952 cisplatin-resistant genes from GeneCards, OMIM, and MsigDB databases. Through Venn diagram analysis, we identified 21 potential therapeutic targets of *S tetrandra* in cisplatin-resistant treatment of OC. Subsequent PPI network construction, cytoscape-based topological analysis, and machine learning algorithms led to the identification of 8 core targets involved in the reversal of cisplatin resistance.

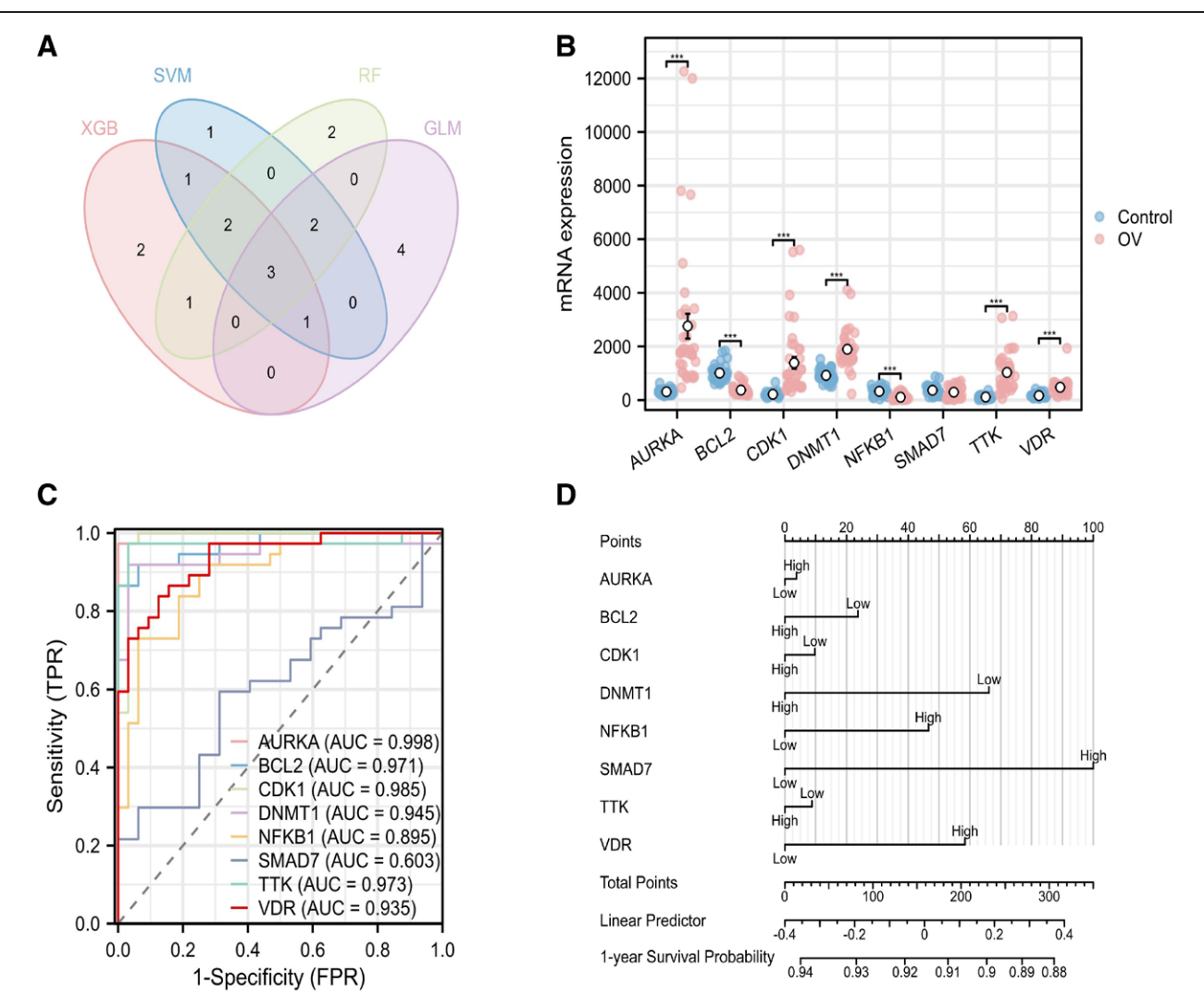


Figure 6. Expression and diagnostic analysis of core targets. (A) Venn diagram of intersecting core genes. (B) Differential expression of core targets between OC and normal groups. (C) ROC curves showing diagnostic performance. (D) Line graphs displaying expression trends of core genes. OC = ovarian cancer, ROC = receiver operating characteristic.

Table 1 Center coordinates of core targets.

Targets name	PDB	Х	γ	Z
TTK	2X9E	-6.774469	21.426163	-0.948041
AURKA	1MQ4	-7.293926	27.375556	80.081778
SMAD7	7CD1	20.434752	2.67417	41.66365
BCL2	1PQ1	0.454225	-7.916631	14.025184
DNMT1	30s5	39.769538	-18.8665	-11.392423
VDR	1DB1	11.4649	22.968	34.461933
NFKB1	1IKN	44.477209	28.034454	3.010969
CDK1	6GU7	33.330846	15.432385	11.445346

 $BCL2 = B-cell \ lymphoma \ 2, CDK1 = cyclin \ dependent \ kinase \ 1, PDB = protein \ data \ bank, TTK = threonine \ tyrosine \ kinase, VDR = vitamin \ D \ receptor.$

Aurora kinases are a family of serine/threonine kinases comprising aurora A (AURKA), aurora B (AURKB), and aurora C (AURKC). Overexpression of AURKA and AURKB has been linked to tumor progression and poor survival outcomes in various cancers. [28] AURKA inhibitors have been found to be potent agents in overcoming cisplatin resistance in tumor cells and tumors. AURKA has been shown to be significantly upregulated in the majority of OC tissues and has an important role in mediating cellular survival after

cisplatin treatment.^[29,30] Its inhibition leads to impaired DNA repair, increased replication stress, and enhanced apoptosis.^[31] Aurora kinase A is essential for cell division, and it serves a critical function in various stages of the mitotic process. AURKA is essential for centrosome maturation, spindle assembly, and accurate chromosome segregation during mitosis, thereby promoting G2/M phase transition and maintaining genomic stability.^[32] Our findings indicated that AURKA was significantly upregulated in OC tissues, which correlated

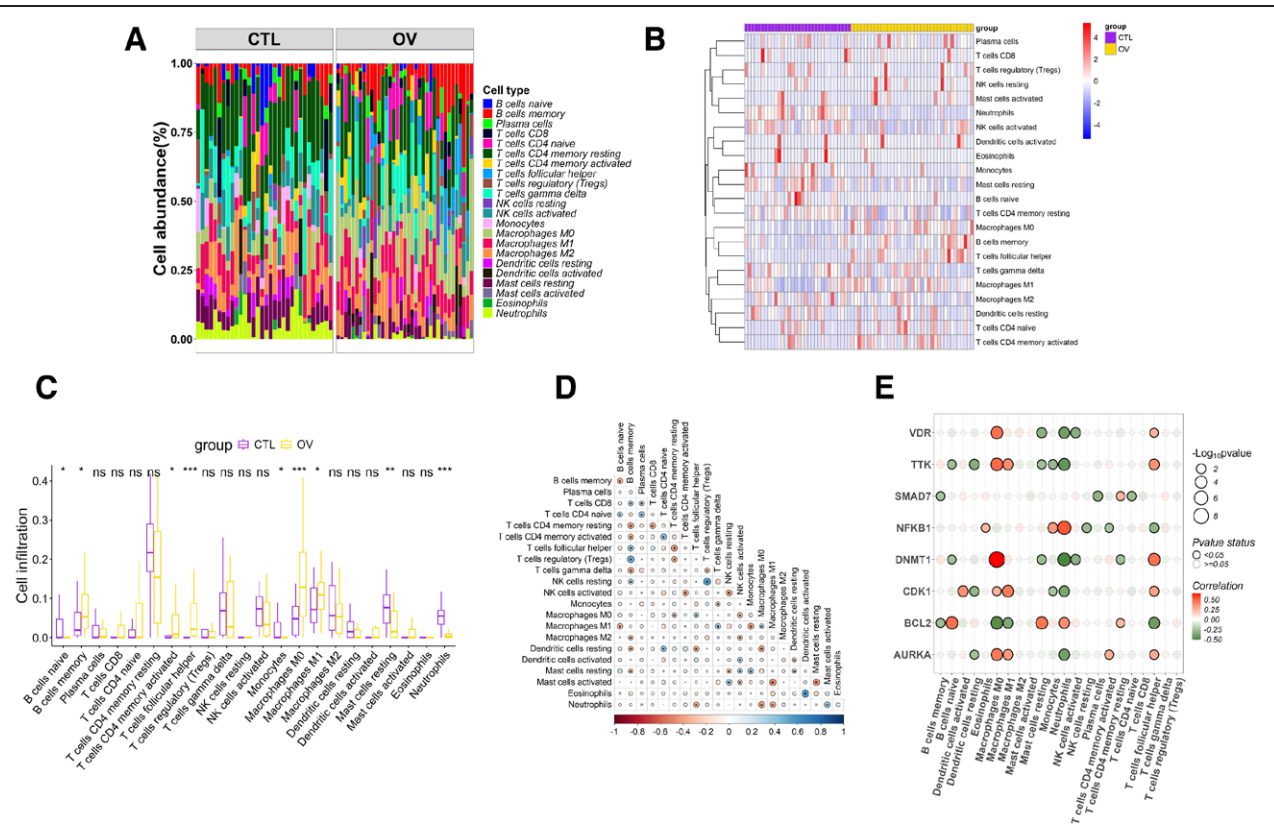


Figure 7. Immune infiltration landscape and its association with core targets. (A) Histogram of immune cell proportions. (B) Heatmap of immune cell expression abundance. (C) Boxplot of immune cell expression. (D) Heatmap of immune cell correlations. (E) Bubble plot showing correlations between core targets and immune cells

with poor prognosis, and inhibition of AURKA enhanced the sensitivity of cancer cells to platinum-based drugs.

TTK, also known as monopolar spindle 1, is a bispecific serine/threonine kinase that plays an important role in the regulation of spindle assembly checkpoint signaling.[33] Spindle assembly checkpoint is a surveillance mechanism during mitosis that ensures the fidelity of chromosome segregation and thus maintains genome stability. Therefore, TTK plays a crucial role in promoting the formation of mitotic checkpoint complexes, facilitating correct chromosome alignment, regulating cell division, and responding to DNA damage. [34] Qi et al found that TTK expression is elevated in cisplatin-resistant OC cell lines such as A2780 and SKOV3 cells, and that proliferation of TTK-knocked-down OC cells was markedly reduced. TTK gene deficiency significantly inhibited cell cycle progression by interfering with the cell cycle progression significantly inhibited the proliferation of OC cells. TTK inhibitors led to increased cisplatin-induced apoptosis and increased sensitivity to cisplatin both in vitro and in vivo.[35]

In this study, NF-κB1 and BCL2 were found to be at the center of the "component-target" network. Among the key regulators of apoptosis, the BCL2 family of proteins plays an important role, and antiapoptotic BCL2 proteins are involved in apoptosis resistance and tumor cell invasion/migration. Chemoresistance data indicate that decreased tumor sensitivity to apoptosis is closely related to drug resistance.^[11] Upregulation of BCL2 is significantly associated with increased chemoresistance.^[36] Nuclear NF-κB1 activates antiapoptotic genes, cell growth factors, multidrug resistance genes, angiogenesis-related genes, and genes related to cell adhesion and metastasis at the transcriptional level, which results in uncontrolled proliferation, apoptotic escape, and drug resistance of malignant cancer cells.^[37] The activation of nuclear NF-κB1 acts as a crucial element in the emergence of apoptotic resistance within malignant cancer

cells. NF-κB1 activation induces the expression of antiapoptotic genes and helps cancer cells to escape cisplatin-induced apoptosis.

KEGG pathway enrichment highlighted significant involvement of the PI3K-AKT signaling pathway, which is hyperactivated in cisplatin-resistant OC. Overactivation of the PI3K/AKT/mTOR pathway is associated with tumor progression, metastasis, and chemoresistance, and it is considered to be a potential prognostic biomarker for patients with OC.^[38] *S tetrandra* components targets act on multiple nodes within this pathway, including NF-κB1 and CCND1, potentially restoring the sensitivity of cancer cells to cisplatin. In the cell cycle pathway, CDK1 and AURKA jointly regulate G2/M progression, their inhibition by *S tetrandra* derivatives may enhance cisplatin-induced cell cycle arrest.

Immune infiltration analysis in this study revealed a positive correlation between AURKA/TTK expression and M0/M1 macrophage infiltration. Given that tumor-associated macrophages promote chemoresistance, targeting these kinases may help reshape the tumor microenvironment.

CDK1 is a central kinase in cell cycle regulation, forming a complex with cell cycle protein B1 (CDK1-cyclin B1) to drive the cell transition from the G2 phase to the M phase. [39] VDR, as a regulator of autophagy, is a ubiquitous nuclear receptor that can regulate the expression of many genes involved in cell differentiation, proliferation, and calcium/phosphate homeostasis. [40] Studies have shown that VDR is a major transcriptional regulator that plays a crucial role in chemosensitivity. [41] *S tetrandra* may have a role in enhancing tumor sensitivity to apoptosis.

Hesperidin is a vitamin P flavonoid compound with antioxidant, anti-inflammatory, and antiapoptotic properties. Hesperidin can alleviate radiation-induced ovarian dysfunction in rats and exhibits significant anti-inflammatory activity by downregulating the expression of ovarian TLR-4, NF-κB,

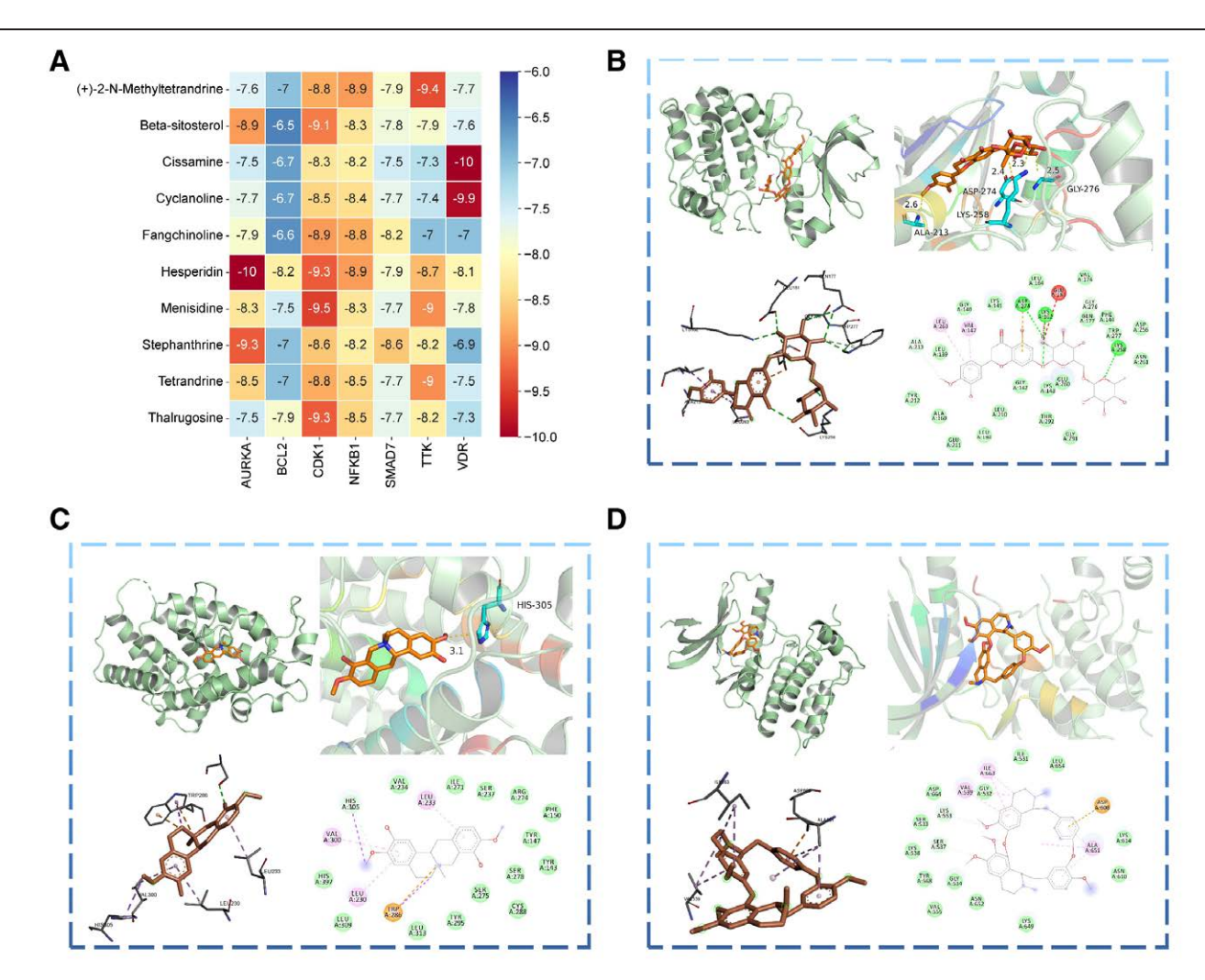


Figure 8. Molecular docking validation of core target and component binding ability. (A) Heatmap of docking binding energies. (B) Interaction mode of AURKA with hesperidin. (C) Interaction mode of VDR with cissamine. (D) Interaction mode of TTK with tetrandrine. TTK = threonine tyrosine kinase.

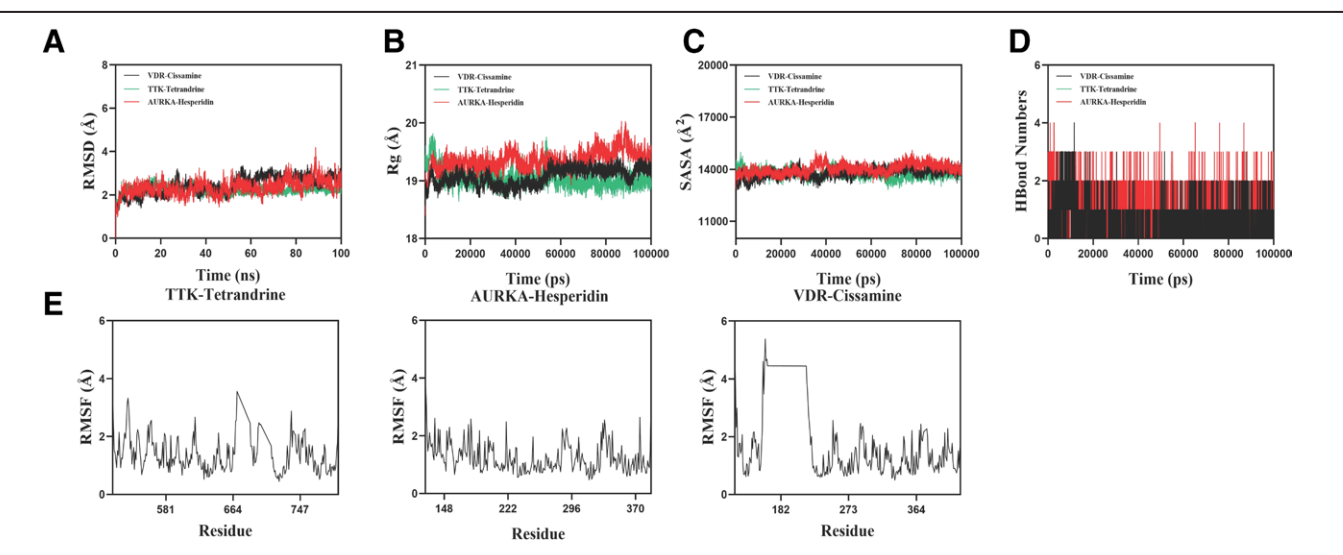


Figure 9. Molecular dynamics simulation of protein-ligand complexes. (A) RMSD values of protein-ligand complexes over time. (B) Rg values of protein-ligand complexes over time. (C) SASA values of protein-ligand complexes over time. (D) HBonds values of protein-ligand complexes over time. (E) RMSF values of protein-ligand complexes. HBonds = hydrogen bonds, Rg = radius of gyration, RMSD = root mean square deviation, RMSF = root mean square fluctuation, SASA = solvent accessible surface area.

and TNF-α.^[42] Zhao et al identified that after treating human OC cells with hesperidin, the viability of A2780 cells decreases in a time- and dose-dependent manner, and apoptosis can be induced.^[43] Li et al demonstrated that cissamine enhances the sensitivity of bladder cancer cells to cisplatin by inhibiting the phosphorylation of JAK2 and STAT3. Cissamine markedly suppresses the proliferation, migration, and invasion of cisplatinresistant bladder cancer cells, promotes apoptosis, and induces cell cycle arrest at the G0/G1 phase.^[44]

Tetrandrine had the widest range of target modulation in this study. It has been reported to synergize with adriamycin in reversing drug resistance in breast cancer cells^[45] and synergistically induce apoptosis, inhibit the proliferation of lung cancer cells in combination with cisplatin. Than the tetrandrine can induce apoptosis in OC cells. Tetrandrine significantly enhances the cell growth inhibition and apoptosis induced by cisplatin, leading to a redistribution of the cell cycle. The Molecular docking confirmed strong binding between TTK and tetrandrine, suggesting its potential role in TTK-mediated resistance via enzymatic inhibition. In summary, through the application of molecular docking and MDS technology, we have provided preliminary evidence to confirm the accuracy of our target predictions.

The identified active components of *S. tetrandra*, particularly tetrandrine, hold promise for clinical translation as adjuvants to overcome cisplatin resistance in OC. However, several formulation challenges must be addressed. Consistent with our ADMET analysis results, tetrandrine exhibit low oral bioavailability due to poor aqueous solubility, which may limit their in vivo efficacy.^[48] Nanoformulation strategies, such as encapsulation in liposomes or polymeric micelles, have shown potential to improve solubility and targeted delivery to tumor tissues.^[49] Additionally, high-dose tetrandrine has been associated with hepatotoxicity in animal models,^[50] necessitating dose optimization and toxicity monitoring in preclinical studies. Future research should focus on developing stable, low-toxicity formulations and evaluating pharmacokinetic profiles in OC models to facilitate clinical translation.

Although this study provides compelling evidence to support the potential of S tetrandra in cisplatin-resistant OC and lays a theoretical foundation for its clinical application, its inherent limitations must be recognized. The reliability of target identification is highly dependent on the accuracy of the database used. In order to improve the effectiveness of the clinical development and application of S tetrandra, rigorous in vitro and in vivo experimental validation is necessary in future studies to confirm our findings. In vitro studies, we will validate the expression of core targets in cisplatin-resistant OC cell lines such as A2780/DDP and SKOV3/DDP by using qPCR and Western blot. Functional experiments including siRNA-mediated knockdown of TTK/AURKA will be performed to assess changes in cell viability, apoptosis, and cisplatin sensitivity via CCK-8 assay and flow cytometry. Additionally, the regulatory effects of key compounds on PI3K-AKT signaling and cell cycle pathways will be verified through Western blot analysis of downstream proteins. In vivo studies, nude mouse xenograft models bearing cisplatin-resistant OC will be used to evaluate the in vivo efficacy of tetrandrine in reversing cisplatin resistance, including tumor growth inhibition and survival rate analysis. Immunohistochemistry will be applied to detect the expression of core targets and pathway-related proteins in tumor tissues. These experiments are designed to confirm the predicted molecular mechanisms and lay a solid foundation for the clinical application of *S tetrandra*.

5. Conclusion

In summary, the present study demonstrated through network pharmacology, bioinformatics analysis, and MDSs that multiple active ingredients – (+)-2-N-methyltetrandrine, hesperidin, menisidine, tetrandrine, and thalrugosine in *S tetrandra* act on key targets involved in OC cisplatin resistance, such as TTK, AURKA, BCL2, VDR, NF-κB, and CDK1. These interactions may modulate the PI3K-AKT signaling pathway, thereby inhibiting cell cycle progression, regulating cell proliferation, and enhancing drug sensitivity. Notably, tetrandrine exhibit the highest number of target interactions, suggesting its considerable potential in preventing and treating cisplatin resistance in OC. This research establishes a robust basis for deeper explorations into the intrinsic mechanisms through which *S tetrandra* exerts its therapeutic effects on OC.

Author contributions

Conceptualization: Yuanyuan Zhong, Shanshan Cai.

Data curation: Chunyue Fang.

Funding acquisition: Yuanyuan Zhong. Methodology: Yuanyuan Zhong, Wei Dai.

Project administration: Wei Dai. Resources: Chunyue Fang. Supervision: Wei Dai.

Software: Yuanyuan Zhong, Shanshan Cai. Visualization: Shanshan Cai, Chunyue Fang. Writing – original draft: Yuanyuan Zhong. Writing – review & editing: Wei Dai.

References

- [1] Huang J, Chan WC, Ngai CH, et al; on behalf of NCD Global Health Research Group of Association of Pacific Rim Universities (APRU). Worldwide burden, risk factors, and temporal trends of ovarian cancer: a global study. Cancers (Basel). 2022;14:2230.
- [2] Wei YF, Ning L, Xu YL, et al. Worldwide patterns and trends in ovarian cancer incidence by histological subtype: a population-based analysis from 1988 to 2017. EClinical Medicine. 2025;79:102983.
- [3] Geng D, Zhou Y, Wang M. Advances in the role of GPX3 in ovarian cancer (Review). Int J Oncol. 2024;64:31.
- [4] Tang C, Xu Z, Duan H, Zhang S. Advancements in artificial intelligence for ultrasound diagnosis of ovarian cancer: a comprehensive review. Front Oncol. 2025;15:1581157.
- [5] Polajžer S, Černe K. Precision medicine in high-grade serous ovarian cancer: targeted therapies and the challenge of chemoresistance. Int J Mol Sci. 2025;26:2545.
- [6] Coleman RL, Fleming GF, Brady MF, et al. Veliparib concomitant with first-line chemotherapy and as maintenance therapy in ovarian cancer: final overall survival and disease-related symptoms results. Eur J Cancer. 2025;225:115587.
- [7] Mombach DM, Mercuri RLV, da Fontoura Gomes TMF, Galante PAF, Loreto ELS. Transposable elements alter gene expression and may impact response to cisplatin therapy in ovarian cancer. Carcinogenesis. 2024;45:685–95.
- [8] Yerrapragada SM, Alex A, Adar S, Kemp MG, Carpenter MA. Treatment of human cells with the anti-cancer drug cisplatin results in the caspase-dependent release of adduct-containing cell-free DNA. DNA Repair (Amst). 2025;151:103855.
- [9] Ma Y, Xue F, Pei Z, Zhao Y. Constructing a co-culture model of cancer-associated fibroblasts and ovarian cancer organoids and studying mechanisms of drug resistance. Exp Cell Res. 2025;450:114656.
- [10] Moore KN, Liu JF, Lorusso D. State of the art: therapies now and around the corner for gynecologic cancers. Am Soc Clin Oncol Educ Book. 2025;45:e473114.
- [11] Yang L, Xie HJ, Li YY, Wang X, Liu XX, Mai J. Molecular mechanisms of platinum-based chemotherapy resistance in ovarian cancer (Review). Oncol Rep. 2022;47:82.
- [12] Lin KH, Tsai CJ, Chen YT, et al. Amentoflavone enhances the antitumor activity of regorafenib by promoting apoptosis and inhibiting NF-κB-mediated metastasis in hepatocellular carcinoma. Anticancer Res. 2025;45:3045–58.
- [13] Palomino GJQ, Celiz HY, Gomes FDR, et al. Withanolide derivatives: natural compounds with anticancer potential offer low toxicity to fertility and ovarian follicles in mice. Anim Reprod. 2024;21:e20240027.

- [14] Koochaki R, Amini E, Zarehossini S, et al. Alkaloids in cancer therapy: targeting the tumor microenvironment and metastasis signaling pathways. Fitoterapia. 2024;179:106222.
- [15] Pasha A, Ravinder D, Pawar SC. Andrographolide mitigates cisplatin resistance by inhibiting SPP1 regulated NF-kB/iNOS/COX-2 and PI3K/ AKT pathway in cisplatin resistant cervical carcinoma cells. Drug Dev Res. 2025;86:e70052.
- [16] Anish Ruban S, Raj FJ, Thangaraj P. Phytochemical intervention in BCRP-driven cancer drug resistance: a comprehensive review. Biochim Biophys Acta Rev Cancer. 2025;1880:189349.
- [17] Jiang Y, Liu M, Liu H, Liu S. A critical review: traditional uses, phytochemistry, pharmacology and toxicology of Stephania tetrandra S. Moore (Fen Fang Ji). Phytochem Rev. 2020;19:449–89.
- [18] Schütz R, Meixner M, Antes I, Bracher F. A modular approach to the bisbenzylisoquinoline alkaloids tetrandrine and isotetrandrine. Org Biomol Chem. 2020;18:3047–68.
- [19] Chu S, Yang W, Lu Y, et al. Tetrandrine inhibits aldosterone synthesis by covalently targeting CYP11A1 to attenuate hypertension. Front Pharmacol. 2024;15:1387756.
- [20] Zhang S, Yan J, Pan W, et al. Assessment of cancer-associated fibroblast signature genes in ovarian cancer patients: impact on immunity, drug resistance, and prognosis. Mol Cell Probes. 2025;83:102038.
- [21] Stelzer G, Rosen N, Plaschkes I, et al. The GeneCards Suite: from gene data mining to disease genome sequence analyses. Curr Protoc Bioinformatics. 2016;54:1.30.1–1.30.33.
- [22] Kong X, Liu C, Zhang Z, et al. BATMAN-TCM 2.0: an enhanced integrative database for known and predicted interactions between traditional Chinese medicine ingredients and target proteins. Nucleic Acids Res. 2024;52:D1110–20.
- [23] Xu HY, Zhang YQ, Liu ZM, et al. ETCM: an encyclopaedia of traditional Chinese medicine. Nucleic Acids Res. 2019;47:D976–82.
- [24] Szklarczyk D, Nastou K, Koutrouli M, et al. The STRING database in 2025: protein networks with directionality of regulation. Nucleic Acids Res. 2025;53:D730–7.
- [25] Jo S, Kim T, Iyer VG, Im W. CHARMM-GUI: a web-based graphical user interface for CHARMM. J Comput Chem. 2008;29:1859–65.
- [26] Wu Y, Yang L, Li Z, Chen Q, Hu J. Polyphyllin VII enhances the antitumor activity of cisplatin in non-small cell lung cancer cells by inducing ferroptosis and enhancing apoptosis. J Biochem Mol Toxicol. 2025;39:e70186.
- [27] Zhang G, Zhang K, Li X, Wang X, Li G, Wang Y. Cinobufagin enhances the sensitivity of cisplatin-resistant lung cancer cells to chemotherapy by inhibiting the PI3K/AKT and MAPK/ERK pathways. J Cell Mol Med. 2025;29:e70501.
- [28] Liu H, Cali Daylan AE, Yang J, et al. Aurora kinase A inhibition potentiates platinum and radiation cytotoxicity in non-small-cell lung cancer cells and induces expression of alternative immune checkpoints. Cancers (Basel). 2024;16:2805.
- [29] Yang H, Ou CC, Feldman RI, Nicosia SV, Kruk PA, Cheng JQ. Aurora-A kinase regulates telomerase activity through c-Myc in human ovarian and breast epithelial cells. Cancer Res. 2004;64:463–7.
- [30] Wang H, Wang Y. Anlotinib induces apoptosis and second growth/mitosis phase block in cisplatin-resistant ovarian cancer cells via the Aurora kinase A/p53 pathway. Hum Exp Toxicol. 2023;42:9603271231185774.
- [31] Li X, Wang Z, Oakley GG, et al. Targeting Aurora A to overcome cisplatin resistance in head and neck cancer. J Dent Res. 2025;104:531–40.

- [32] Willems E, Dedobbeleer M, Digregorio M, Lombard A, Lumapat PN, Rogister B. The functional diversity of Aurora kinases: a comprehensive review. Cell Div. 2018;13:7.
- [33] Liu X, Winey M. The MPS1 family of protein kinases. Annu Rev Biochem. 2012;81:561–85.
- [34] Lima I, Borges F, Pombinho A, Chavarria D. The spindle assembly checkpoint: molecular mechanisms and kinase-targeted drug discovery. Drug Discov Todav. 2025;30:104355.
- [35] Qi G, Ma H, Li Y, Peng J, Chen J, Kong B. TTK inhibition increases cisplatin sensitivity in high-grade serous ovarian carcinoma through the mTOR/autophagy pathway. Cell Death Dis. 2021;12:1135.
- [36] Li Z, Wu YH, Guo YQ, Min XJ, Lin Y. Tasquinimod promotes the sensitivity of ovarian cancer cells to cisplatin by down-regulating the HDAC4/p21 pathway. Korean J Physiol Pharmacol. 2025;29:191–204.
- [37] Xin L, Yang WF, Zhang HT, Li YF, Liu C. The mechanism study of lentiviral vector carrying methioninase enhances the sensitivity of drug-resistant gastric cancer cells to Cisplatin. Br J Cancer. 2018;118:1189–99.
- [38] Zheng K, Jin G, Cao R, et al. Targeting on the PI3K/mTOR: a potential treatment strategy for clear cell ovarian carcinoma. Cancer Chemother Pharmacol. 2025;95:21.
- [39] Lei X, Wang Y, Chen Y, Duan J, Gao X, Cong Z. Fenbendazole exhibits antitumor activity against cervical cancer through dual targeting of cancer cells and cancer stem cells: evidence from in vitro and in vivo models. Molecules. 2025;30:2377.
- [40] Sun J. VDR/vitamin D receptor regulates autophagic activity through ATG16L1. Autophagy. 2016;12:1057–8.
- [41] Koll L, Gül D, Elnouaem MI, et al. Exploiting vitamin D receptor and its ligands to target squamous cell carcinomas of the head and neck. Int J Mol Sci. 2023;24:4675.
- [42] Mohamed DH, Said RS, Kassem DH, Gad AM, El-Demerdash E, Mantawy EM. Hesperidin attenuates radiation-induced ovarian failure in rats: emphasis on TLR-4/NF-κB signaling pathway. Toxicol Appl Pharmacol. 2024;492:117111.
- [43] Zhao J, Li Y, Gao J, De Y. Hesperidin inhibits ovarian cancer cell viability through endoplasmic reticulum stress signaling pathways. Oncol Lett. 2017;14:5569–74.
- [44] Li L, Li C, Miao F, et al. Cyclanoline reverses cisplatin resistance in bladder cancer cells by inhibiting the JAK2/STAT3 pathway. Anticancer Agents Med Chem. 2024;24:1360–70.
- [45] Xin G, Hou Y, Liu Y, Li H. Tetrandrine and adriamycin reverse multidrug resistance by regulating NLRP3/Caspase-1/GSDMD signaling in human breast cancer cells. Eur J Pharmacol. 2025;998:177635.
- [46] Ye LY, Hu S, Xu HE, et al. The effect of tetrandrine combined with cisplatin on proliferation and apoptosis of A549/DDP cells and A549 cells. Cancer Cell Int. 2017;17:40.
- [47] Zhang Y, Wang C, Wang H, Wang K, Du Y, Zhang J. Combination of Tetrandrine with cisplatin enhances cytotoxicity through growth suppression and apoptosis in ovarian cancer in vitro and in vivo. Cancer Lett. 2011;304:21–32.
- [48] Xue F, Yang L, Ma S, et al. Preparation and evaluation of tetrandrine nanocrystals to improve bioavailability. Curr Drug Deliv. 2025;22:648–57.
- [49] Ling J, Wu J, Cao Y, et al. Advances in nano-preparations for improving tetrandrine solubility and bioavailability. Arch Pharm (Weinheim). 2024;357:e2400274.
- [50] Qi XM, Miao LL, Cai Y, Gong LK, Ren J. ROS generated by CYP450, especially CYP2E1, mediate mitochondrial dysfunction induced by tetrandrine in rat hepatocytes. Acta Pharmacol Sin. 2013;34:1229–36.